DOI: 10.1002/((please add manuscript number))

Article type: Communication

A New Design Strategy for Efficient Thermally Activated Delayed Fluorescence (TADF) Organic Emitters: From Twisted to Planar Structures

*Xian-Kai Chen, Youichi Tsuchiya, Yuma Ishikawa, Cheng Zhong, Chihaya Adachi, and Jean-Luc Brédas**

Dr. X.-K. Chen, Dr. C. Zhong, Prof. J.-L. Brédas

Laboratory for Computational and Theoretical Chemistry of Advanced Materials

Division of Physical Science and Engineering

King Abdullah University of Science and Technology

Thuwal 23955-6900, Saudi Arabia.

Dr. X.-K. Chen, Prof. J.-L. Brédas

New permanent address: School of Chemistry and Biochemistry, Georgia Institute of Technology, Atlanta, Georgia 30332-0400

Dr. C. Zhong

New permanent address: Department of Chemistry, Wuhan University, Wuhan, 430072, China

* Corresponding author: jean-luc.bredas@chemistry.gatech.edu

Prof. Y. Tsuchiya, Mr. Y. Ishikawa, Prof. C. Adachi

Center for Organic Photonics and Electronics Research (OPERA), Kyushu University,

744 Motooka, Nishi, Fukuoka 819-0395, Japan.

Prof. Y. Tsuchiya, Prof. C. Adachi

Japan Science and Technology Agency (JST), ERATO, Adachi Molecular Exciton Engineering Project, 744 Motooka, Nishi, Fukuoka 819-0395, Japan.

Prof. C. Adachi

International Institute for Carbon Neutral Energy Research (WPI-I2CNER), Kyushu University, 744 Motooka, Nishi, Fukuoka 819-0395, Japan.

Keywords: thermally activated delayed fluorescence, molecular design, singlet-triplet energy gap, oscillator strength, coplanar structure

Abstract

In the traditional molecular design of thermally activated delayed fluorescence (TADF) emitters composed of electron-donor and electron-acceptor moieties, achieving a small singlet-triplet energy gap (ΔE_{ST}) in strongly twisted structures usually translates into a small fluorescence oscillator strength, which can significantly decrease the emission quantum yield and limit efficiency in organic light-emitting diode (OLED) devices. Here, based on the results of quantum-chemical calculations on TADF emitters composed of carbazole donor and 2,4,6-triphenyl-1,3,5-triazine acceptor moieties, we propose a new strategy for the molecular design of efficient TADF emitters that combine a small ΔE_{ST} with a large fluorescence oscillator strength. Since this strategy goes beyond the traditional framework of structurally twisted, charge-transfer type emitters, importantly, it opens the way for coplanar molecules to be efficient TADF emitters. Here, we have theoretically designed the HMAT-TRZ emitter, composed of azatriangulene and diphenyltriazine moieties, which is coplanar due to

intra-molecular H-bonding interactions. The synthesis of HMAT-TRZ and its preliminary photophysical characterizations point to HMAT-TRZ as a potential efficient TADF emitter.

In the field of organic light-emitting diodes (OLEDs), much attention has been recently given to efficient harvesting of triplet excitons via reverse intersystem crossing (RISC) from the lowest triplet (T_1) excited state to the lowest singlet (S_1) excited state, induced by thermal activation.[1] This process gives rise to thermally activated delayed fluorescence (TADF), with the singlet exciton yields greatly exceeding the theoretical limit (*i.e.*, 25%) derived from spin statistics, which can lead to internal quantum efficiencies near 100% in metal-free organic compounds.[1] Purely organic TADF emitters thus represent a promising pathway towards high-performance and low-cost full-color and white OLEDs.

Small singlet-triplet energy gaps (ΔE_{ST}) are required to facilitate the $T_1 \rightarrow S_1$ RISC process in TADF emitters.[2-4] Early investigations on TADF systems have been based on the premise that a small ΔE_{ST} can be achieved by separating the wavefunction distributions of the highest occupied molecular orbitals (HOMOs) and lowest unoccupied molecular orbitals (LUMOs).[5-8] This initial molecular-design strategy relies on the simple principle that, if the main electron configuration describing both the S_1 and T_1 states corresponds to such a HOMO-to-LUMO transition (*i.e.*, a single electron-configuration description), the exchange energy will vanish and ΔE_{ST} will be very small. In this

instance (here, in the context of linear response time-dependent density functional theory (LR-TDDFT) under the Tamm-Dancoff approximation (TDA)),[9] ΔE_{ST} can be expressed as:

$$\Delta E_{ST} = 2\left(\mathrm{HOMO}(1)\mathrm{LUMO}(1)|\, f_{Hxc} \,|\, \mathrm{LUMO}(2)\mathrm{HOMO}(2)\right) \quad (1)$$

where f_{Hxc} denotes the Coulomb-exchange-correlation kernel. According to Equation (1), ΔE_{ST} is directly proportional to the overlap (<H|L>; H: HOMO and L: LUMO) between the HOMO and LUMO wavefunctions. Based on this single electron-configuration recipe, a number of TADF emitters with small or even vanishing ΔE_{ST} have been found in highly twisted molecules composed of electron-donor (D) and electron-acceptor (A) moieties.[2-4] In such molecules, both S_1 and T_1 states have a substantial charge-transfer (CT) excitation character. However, in such CT molecules, the transition dipole moments $\mu_{S_1-S_0}$ between the ground state (S_0) and the S_1 state are expected to be very small since $\mu_{S_1-S_0}$ is also directly proportional to the HOMO-LUMO orbital overlap:

$$\mu_{S_1-S_0} = \left|\left\langle \Psi_{S_1} \left|\bar{\mu}\right| \Psi_{S_0} \right\rangle\right| \approx \left|\left\langle L \left|\bar{\mu}\right| H \right\rangle\right| \propto \left|\left\langle L \left| H \right\rangle\right| \quad (2)$$

where $\bar{\mu}$ denotes the dipole operator and Ψ_{S_0/S_1}, the electronic wavefunctions of the S_0/S_1 state. As a consequence, while TADF emitters with such a CT excitation character can present an almost vanishing singlet-triplet energy gaps and thus a fast RISC rate, the weakness of the $S_1 \rightarrow S_0$ transition dipole moments (and therefore of the oscillator strength that depends on $\left|\mu_{S_1-S_0}\right|^2$) can significantly decrease the photoluminescence quantum yield (PLQY), and limit efficiencies in OLED devices.[10, 11] [12, 13]

Recently, some of us have synthesized and characterized TADF emitters composed of carbazole donor and 2,4,6-triphenyl-1,3,5-triazine acceptor moieties,[11] see the CPT2 – CPT4 series in **Figure 1a**; these emitters have shown very good photophysical properties and device performance. In particular, the CPT3 and CPT4 molecular systems not only have large oscillator strengths for fluorescence radiative decay, leading to PLQYs of nearly 100%, but also moderate ΔE_{ST} values (lower than 0.3 eV), with the result that external electroluminescent quantum efficiencies of the OLED devices reach up to 20%.[11] In addition, it was found experimentally that an increase in the number of carbazole donors led to an increase in the fluorescence oscillator strength and a decrease in singlet-triplet energy gap. These findings, however, cannot be rationalized on the basis of the traditional design principle of CT molecules. Thus, it is critical to develop more reliable descriptions of the microscopic mechanisms behind a combination of large fluorescence oscillator strength and small ΔE_{ST}.

Here, we first consider the CPT1 − CPT4 series shown in Figure 1a, and analyze the electronic structures of their S_1 and T_1 states via advanced quantum-chemical (QC) calculations; we focus on the (vertical and adiabatic) excitation energies, natural transition orbitals (NTO) describing the S_1 and T_1 excitations,[14] and overlaps of the corresponding electron-hole density distributions (the computational methodologies are detailed in Part A of the Supporting Information (SI)). For the sake of comparison, CPT5 with strongly electron-donating N,N-dimethyl groups, see Figure 1a, is also investigated. The results of the calculations allow us to rationalize the mechanism behind the efficiency of these TADF emitters. Importantly, they allow us to propose a new molecular-design strategy that can be extended to *coplanar* TADF emitters.

For the CPT1 – CPT4 systems, the calculations indicate that an increase in the number of donor moieties leads to a decrease in the $S_0 \rightarrow S_1$ (both vertical and adiabatic) excitation energies while the $S_0 \rightarrow T_1$ excitation energies hardly change, see Figure 1b; therefore, the singlet-triplet energy gaps reduce.[15] To better understand the natures of the S_1 and T_1 excited states, it is useful to refer to the NTO analysis, see **Figure 2a**. We note that, for the S_1 states, the NTO hole and electron wavefunctions mainly distribute on the carbazole donor and triazine acceptor moieties, respectively, but overlap on the phenylene bridges; thus, the S_1 states have a hybrid character combining local and charge-transfer excitations; with an increase in the number of donor moieties, the hole tends to delocalize more on these moieties in order to stabilize the S_1 states. The relationships between molecular architectures and S_1 states with a hybrid excitation character also have been experimentally studied in other twisted D-A molecules.[16]

For the T_1 states, interestingly, the hole and electron wavefunctions are confined on the central carbazole-phenylene-triazine molecular fragment. This confinement is not altered in the presence of more functional groups, which is the reason why the T_1 excitation energies hardly change along the series. To better assess the characteristics of the S_1 and T_1 states, Figure 2b collects the dihedral angles between the donor and bridge-acceptor moieties in the optimized S_1 and T_1 geometries, while Figure 2c displays the overlaps between the hole and electron (h/e) density distributions in the S_1 and T_1 states. Compared to CPT1, the presence of additional donor moieties in the CPT2 – CPT4 series leads to an increase in donor–[bridge-acceptor] dihedral angles and a decrease in the h-e overlaps for the S_1 states, which is consistent with the results of the NTO analysis. For the T_1 states, the donor–[bridge-acceptor] dihedral angles and h-e overlaps do not change and remain at values of *ca.* 45º and 0.5, respectively, along the series. It is useful to note that the

dihedral angles between phenylene bridge and triazine acceptor are zero in all the molecules studied here due to H-bonding interactions between the two fragments.

The reason for the confinement of the T_1 exciton wavefunctions of the CPT1 – CPT4 molecules on the central carbazole-phenylene-triazine fragment can be found by: (i) inspecting the T_1-state energies of the carbazole and phenylene-triazine fragments based on the T_1 equilibrium geometry of the CPT1; and (ii) performing a NTO analysis, see **Figure 3**. The T_1 energies of the two fragments are in fact nearly identical, *ca.* 3.5 eV (a value in agreement with the results of other high-level QC calculations).[17] In addition, the NTO hole and electron wavefunctions have large distributions on the atoms linking the two fragments (see Figure 3b). The combination of these two factors gives rise to a large electronic coupling (~ 1.1 eV) between the T_1 states of the two fragments, which results in a low T_1 energy (~ 2.4 eV) for the central fragment. As a consequence, when additional carbazole moieties that individually have a high triplet energy are introduced, the T_1 energies and wavefunctions along the CPT2 – CPT4 series are not impacted.

At this stage, two main points can be summarized:

(i) The T_1 wavefunctions in the CPT1 – CPT4 series are confined to the carbazole-phenylene-triazine fragment due to the low triplet energy coming from the large electronic coupling between the carbazole and phenylene-triazine moieties.

(ii) The additional carbazole donors into the CPT1 decreases the S_1-state energies in the CPT2 – CPT4 series, but has hardly any impact on the T_1-state energies and wavefunctions, which results in a reduction of the singlet-triplet energy gaps. This combination of effects can be taken as a new strategy in order to minimize the singlet-triplet energy gaps in organic D-A molecules.

To further test the validity of this strategy, we have designed the CPT5 molecule that has additional strongly electron-donating N,N-dimethyl groups. The calculated S_1 and T_1 excitation energies are shown in Figure 1b. Compared to CPT1, the S_1-state adiabatic excitation energy in CPT5 decreases significantly, by 0.96 eV, while the T_1 energy reduces much less, by *ca.* 0.4 eV; as a result, the ΔE_{ST} in CPT5 is nearly zero. The NTO analysis of CPT5 confirms that the S_1 state has CT-excitation character while the T_1 exciton wavefunction remains confined on the central fragment, which is consistent with a local excitation character of the T_1 state, see Figure 2a. We recall that in the traditional CT molecular-design strategy, a vanishing ΔE_{ST} can be achieved only in the situation where both the S_1 and T_1 states have substantial CT excitation character. Therefore, our results for CPT5 demonstrate that the strategy developed here to reduce ΔE_{ST} is markedly different. In addition, our new design overcomes the conflict stemming from the usual opposite trends in ΔE_{ST} and $S_1 \rightarrow S_0$ transition dipole moment, which is critical for efficient TADF emitters.

To illustrate the advantage of the new strategy in maintaining large S_0-S_1 transition dipole moments (and fluorescence oscillator strengths), it is relevant to analyze further the electronic structure of the S_1 states in the CPT1 – CPT4 series, see **Table 1**. The results underline that the transition dipole moments in these molecules are very large, up to ~ 7 Debye, *i.e.*, much larger than in traditional CT TADF emitters. From Table 1, we note that:

(i) The main electron configuration describing the S_1 state corresponds to the HOMO → LUMO transition.

(ii) In going from CPT1 to CPT2, the introduction of the additional carbazole donor reduces the contribution of the HOMO → LUMO electron configuration to the S_1 state, as well as the HOMO-LUMO orbital overlap due to the delocalization of the HOMO wavefunction on the additional

carbazole (see Figure S2 in the SI), which decreases the transition dipole moment. While the HOMO-1 → LUMO transition also has a contribution to the S_1 state in CPT2, the orbital overlap between the HOMO-1 and LUMO levels is very small (~ 0.04), which means that this electron configuration has very little impact on the transition dipole moment.

(iii) In going from CPT2 to CPT3, the additional carbazole has almost no impact on the contribution of the HOMO → LUMO electron configuration to the S_1 state and the HOMO-LUMO overlap. Interestingly, the HOMO-4 → LUMO electron configuration appears in the description of the S_1 state and has significant orbital overlap (~ 0.33), which enhances the transition dipole moment. It is this HOMO-4 → LUMO electron configuration that contributes to the increase in the hole-electron density overlap in the S_1 state of CPT3, as shown in Figure 2c. Thus, on the basis of the CPT1 carbazole-phenylene-triazine fragment, the introduction of multiple π-conjugated carbazole donors not only reduces the singlet-triplet energy gaps, but also maintains large transition dipole moments (due to the contributions of multiple electronic configurations), which allows one to understand the efficiency of the CPT3 and CPT4 TADF emitters. It may be the reason why many high-efficiency TADF emitters in fact contain multiple π-conjugated donor moieties.[18-21]

In addition to twisted molecules, the new molecular-design strategy can be extended to *coplanar* TADF emitters. An example is given by HMAT-TRZ, which is composed of azatriangulene and diphenyltriazine moieties, see **Figure 4a**. The calculations indicate that the ground-state geometry of HMAT-TRZ is nearly coplanar due to the H-bonding interactions between azatriangulene and diphenyltriazine, although the azatriangulene group slightly buckles (see Figure 4b). We note that the coplanarity of HMAT-TRZ predicted by the calculations is supported by experimental data

on HMAT and a number of its derivatives, which have been reported to be (nearly) coplanar via single crystal X-ray diffraction.[22-26]

As we would have expected on the basis of our earlier arguments, the $S_1 \rightarrow S_0$ transition dipole moment is very large, about 10 Debye, due to the large NTO hole-electron overlap favored by the coplanar molecular structure in the S_1 state (see Figure 4b). In the T_1 state, the hole and electron wavefunctions are also confined to the central molecular region (the NTO orbitals are illustrated in Figure S3 in the SI). The calculated ΔE_{ST} is relatively large, *ca.* 0.43 eV; however, as detailed above, we can apply the strategy of introducing multiple donor moieties (*e.g.*, methoxy-diphenylamine groups) to further reduce ΔE_{ST} while maintaining a large fluorescence oscillator strength, see Figure S4 in the SI.

To verify whether HMAT-TRZ is a potential efficient TADF emitter, we conducted its synthesis and preliminary photophysical characterizations (the experimental details are given in Part B of the SI). Figures 4c and S5 show the absorption and emission spectra of HMAT-TRZ in various polar and nonpolar solvents. We find that the nature of the solvent has little impact on the absorption spectra; compared to typical twisted TADF emitters,[6, 27] HMAT-TRZ shows a much stronger absorption and its molar absorption coefficient is up to ca. 4.3×10^4 L mol^{-1} cm^{-1}, which is consistent with the fact that the ground-state geometry of HMAT-TRZ is more coplanar. With an increase in solvent polarity, the emission spectra red-shift and broaden while the vibronic structure disappears, which implies an increasing contribution of CT character in the relaxed S_1-state excitation (see Figure S5 in the SI). Figure 4d presents the transient photoluminescence decay spectra for a polymethylmethacrylate (PMMA) film doped with 10 mol% HMAT-TRZ, under vacuum and ambient conditions; Figure S6 (in the SI) shows the transient PL decay images obtained from streak camera measurements. Delayed

fluorescence is clearly found in the doped film at 300 K, with an emission wavelength of *ca.* 500 nm (see Figure 4c); a longer lifetime of the delayed component (τ_{d1} = 0.67 ms, τ_{d2} = 4.44 ms) is obtained under vacuum, compared to ambient conditions. At 10 K, the delayed component diminishes significantly and the emission is then identified as phosphorescence at a longer wavelength of *ca.* 550 nm, see Figure S6.

In addition, other host matrixes, *e.g.,* 3,3-di(9H-carbazol-9-yl)biphenyl (mCBP) and bis[2-(diphenylphosphino)phenyl]ether oxide (DPEPO), were also used to disperse the HMAT-TRZ guest; the photophysical parameters of the corresponding doped films are listed in Table S1 (see the SI). We find that the doped mCBP film shows good photophysical performance, with a high PLQY of 84.7% under argon (75.8% under ambient condition). From the streak image shown in **Figure 5a**, delayed fluorescence is clearly observed at 300 K, with a long lifetime of the delayed component (τ_{d1} = 0.70 ms and τ_{d2} = 7.18 ms in vacuo, corresponding to 21.5% and 78.5% of the whole delayed component, respectively), similar to the doped PMMA film. The second-order decay evolution in the delayed component should be ascribed to the formation of HMAT-TRZ aggregates in the 10 wt% HMAT-TRZ doped mCBP film. Compared to the 10 wt% doped mCBP, the delayed fluorescence lifetime and PLQY of HMAT-TRZ decrease in the 20 wt% doped sample (see Table S1 and Figure S8 in the SI), which again can be attributed to molecular aggregation of HMAT-TRZ. As reported in previous investigations[28, 29], the photo-physical properties of TADF emitters are susceptible to the choice of medium and doping concentrations, with HMAT-TRZ in different hosts (*e.g.*, mCBP, DPEPO, or PMMA) showing very different fluorescence decay behaviors (see Table S1 and Figure S8 in the SI). The temperature dependence of the transient photoluminescence decay spectra is shown in Figure 5b. We find that the delayed component decreases when lowering temperature and

completely disappears below 200 K (see Figure 5b). Figure 5c shows that the delayed fluorescence spectra at 300 and 250 K are very similar to the prompt component spectrum; below 100 K, the red-shifted emission is identified as phosphorescence; at 200 K, the delayed component contains both delayed fluorescence and phosphorescence. Taken together, these experimental results point to HMAT-TRZ as a potential efficient TADF emitter, and indicate that the mCBP host can provide an appropriate environment for the generation of TADF.

It is worth stressing that the transient spectral studies give a ΔE_{ST} estimate of ~ 0.38 eV, which is substantially larger than in other reported TADF materials (< 0.3 eV). As we described above, in the framework of the molecular-design strategy presented here, the introduction of multiple donor moieties (*e.g.*, methoxy-diphenylamine groups) could further reduce ΔE_{ST} while maintaining a large fluorescence oscillator strength (as illustrated in Figure S4 in the SI). In addition, other factors, *e.g.*, spin-orbit coupling (SOC) between the S_1 and T_1 states[15] and non-adiabatic coupling between low-lying excited states,[30, 31] also play important roles in the $T_1 \rightarrow S_1$ reverse intersystem crossing for TADF emitters. More detailed investigations of RISC mechanism in planar TADF emitters are definitely warranted.

To conclude, based on the results of quantum-chemical calculations on TADF emitters composed of carbazole donor and 2,4,6-triphenyl-1,3,5-triazine acceptor moieties, we proposed a new strategy for the molecular design of efficient TADF emitters that combine a small ΔE_{ST} with a large fluorescence oscillator strength. This strategy goes beyond the traditional framework of twisted CT-type TADF molecular design. The key in the strategy developed here is that the S_1-state energies in these molecules reduce with an increase in the number of carbazole donors, due to wavefunction delocalization, while the T_1-state energies hardly evolve, due to the confinement of

the T_1-state wavefunction on the central carbazole-phenylene-triazine fragment that has a lower T_1 energy. The net result is to reduce the singlet-triplet energy gaps. At the same time, the introduction of multiple carbazole donors onto the carbazole-phenylene-triazine fragment helps maintain a large $S_1 \rightarrow S_0$ transition dipole moment due to contributions of multiple electronic configurations that have large relevant orbital overlaps.

In addition to twisted molecules, the strategy detailed here can be applied to the molecular design of *coplanar* TADF emitters. We have designed, at the theoretical level, the HMAT-TRZ emitter, which is coplanar due to intra-molecular H-bonding interactions. The synthesis of HMAT-TRZ and its photo-physical characterizations point to HMAT-TRZ as a potential, efficient TADF emitter. Finally, we note that the present molecular design is not limited to helping the development of efficient TADF emitters for OLED applications; it can also be useful in the development of donors and acceptors with T_1-state energies close to S_1-state energies, in order to suppress triplet exciton formation via bimolecular recombination in organic solar-cell devices.[32, 33]

Supporting Information

Supporting Information is available from the Wiley Online Library or from the authors.

Acknowledgements

X.-K. Chen, C. Zhong, and J.L. Bredas thank King Abdullah University of Science and Technology (KAUST) for generous research funding as well as the KAUST IT Research Computing Team and the

Supercomputing Laboratory for providing continuous assistance as well as computational and storage resources. This work was supported in part by Exploratory Research for Advanced Technology (ERATO, JPMJER1305) from Japan Science and Technology Agency (JST).

Received: ((will be filled in by the editorial staff))
Revised: ((will be filled in by the editorial staff))
Published online: ((will be filled in by the editorial staff))

References

[1] H. Uoyama, K. Goushi, K. Shizu, H. Nomura, C. Adachi, *Nature* **2012**, *492*, 234.

[2] A. Chihaya, *Jpn. J. Appl. Phys.* **2014**, *53*, 060101.

[3] Y. Tao, K. Yuan, T. Chen, P. Xu, H. Li, R. Chen, C. Zheng, L. Zhang, W. Huang, *Adv. Mater.* **2014**, *26*, 7931.

[4] Z. Yang, Z. Mao, Z. Xie, Y. Zhang, S. Liu, J. Zhao, J. Xu, Z. Chi, M. P. Aldred, *Chem. Soc. Rev.* **2017**, *46*, 915.

[5] H. Tanaka, K. Shizu, H. Miyazaki, C. Adachi, *Chem. Commun.* **2012**, *48*, 11392.

[6] Q. Zhang, B. Li, S. Huang, H. Nomura, H. Tanaka, C. Adachi, *Nat Photon* **2014**, *8*, 326.

[7] K. Goushi, K. Yoshida, K. Sato, C. Adachi, *Nat. Photon.* **2012**, *6*, 253.

[8] Q. Zhang, J. Li, K. Shizu, S. Huang, S. Hirata, H. Miyazaki, C. Adachi, *J. Am. Chem. Soc.* **2012**, *134*, 14706.

[9] M. E. Casida, M. Huix-Rotllant, *Annu. Rev. Phys. Chem.*, **2012**, *63*, 287.

[10] K. Sato, K. Shizu, K. Yoshimura, A. Kawada, H. Miyazaki, C. Adachi, *Phys. Rev. Lett.* **2013**, *110*, 247401.

[11] S. Hirata, Y. Sakai, K. Masui, H. Tanaka, S. Y. Lee, H. Nomura, N. Nakamura, M. Yasumatsu, H. Nakanotani, Q. Zhang, K. Shizu, H. Miyazaki, C. Adachi, *Nat. Mater.* **2015**, *14*, 330.

[12] M. Y. Wong, E. Zysman-Colman, *Adv. Mater.* **2017**, *29*, 1605444.

[13] M. Godumala, S. Choi, M. J. Cho, D. H. Choi, *J. Mater. Chem. C* **2016**, *4*, 11355.

[14] R. L. Martin, *J. Chem. Phys.* **2003**, *118*, 4775.

[15] P. K. Samanta, D. Kim, V. Coropceanu, J.-L. Brédas, *J. Am. Chem. Soc.* **2017**, *139*, 4042.

[16] S. Zhang, L. Yao, Q. Peng, W. Li, Y. Pan, R. Xiao, Y. Gao, C. Gu, Z. Wang, P. Lu, F. Li, S. Su, B. Yang, Y. Ma, *Adv. Funct. Mater.* **2015**, *25*, 1755.

[17] M. Pabst, D. Sundholm, A. Köhn, *J. Phys. Chem. C* **2012**, *116*, 15203.

[18] C. Mayr, S. Y. Lee, T. D. Schmidt, T. Yasuda, C. Adachi, W. Brütting, *Adv. Funct. Mater.* **2014**, *24*, 5232.

[19] T. Takehiro, S. Katsuyuki, Y. Takuma, T. Kazunori, A. Chihaya, *Sci. Technol. Adv. Mat.* **2014**, *15*, 034202.

[20] H. Kaji, H. Suzuki, T. Fukushima, K. Shizu, K. Suzuki, S. Kubo, T. Komino, H. Oiwa, F. Suzuki, A. Wakamiya, Y. Murata, C. Adachi, *Nat. Commun.* **2015**, *6*, 8476.

[21] K. Albrecht, K. Matsuoka, K. Fujita, K. Yamamoto, *Angew. Chem. Int. Ed.* **2015**, *54*, 5677.

[22] Z. Fang, X. Zhang, Y. Hing Lai, B. Liu, *Chem. Commun.* **2009**, 920.

[23] U. Meinhardt, F. Lodermeyer, T. A. Schaub, A. Kunzmann, P. O. Dral, A. C. Sale, F. Hampel, D. M. Guldi, R. D. Costa, M. Kivala, *RSC Adv.* **2016**, *6*, 67372.

[24] Z. Fang, V. Chellappan, R. D. Webster, L. Ke, T. Zhang, B. Liu, Y.-H. Lai, *J. Mater. Chem.* **2012**, *22*, 15397.

[25] Z. Fang, T.-L. Teo, L. Cai, Y.-H. Lai, A. Samoc, M. Samoc, *Org. Lett.* **2009**, *11*, 1.

[26] Z. Jiang, Y. Chen, C. Yang, Y. Cao, Y. Tao, J. Qin, D. Ma, *Org. Lett.* **2009**, *11*, 1503.

[27] K. Nasu, T. Nakagawa, H. Nomura, C.-J. Lin, C.-H. Cheng, M.-R. Tseng, T. Yasuda, C. Adachi, *Chem. Commun.* **2013**, *49*, 10385.

[28] G. Méhes, K. Goushi, W. J. Potscavage, C. Adachi, *Org. Electron.* **2014**, *15*, 2027.

[29] B. D. Fernando, J. P. Thomas, P. M. Andrew, *Methods Appl. Fluoresc.* **2017**, *5*, 012001.

[30] X.-K. Chen, S.-F. Zhang, J.-X. Fan, A.-M. Ren, *J. Phys. Chem. C* **2015**, *119*, 9728.

[31] M. K. Etherington, J. Gibson, H. F. Higginbotham, T. J. Penfold, A. P. Monkman, *Nat. Commun.* **2016**, *7*, 13680.

[32] P. C. Y. Chow, S. Gélinas, A. Rao, R. H. Friend, *J. Am. Chem. Soc.* **2014**, *136*, 3424.

[33] A. Rao, P. C. Y. Chow, S. Gelinas, C. W. Schlenker, C.-Z. Li, H.-L. Yip, A. K. Y. Jen, D. S. Ginger, R. H. Friend, *Nature* **2013**, *500*, 435.

(a)

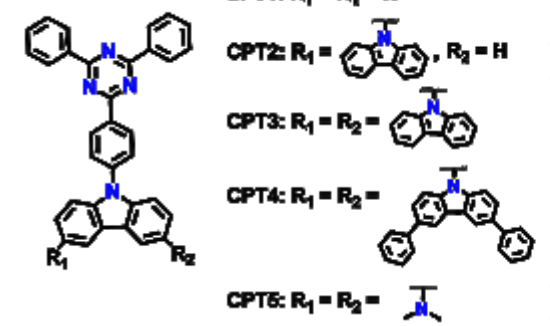

(b)

	$E_v(S_0\text{-}S_1)$	$E_a(S_0\text{-}S_1)$	$E_v(S_0\text{-}T_1)$	$E_a(S_0\text{-}T_1)$	ΔE_{ST}
CPT1	3.48	3.27	3.07	2.73	0.54
CPT2	3.46 (3.38)	3.15	3.08	2.74 (2.75)	0.41 (0.32)
CPT3	3.45 (3.37)	3.14	3.10	2.75 (2.75)	0.39 (0.28)
CPT4	3.41 (3.42)	3.10	3.10	2.75	0.35
CPT5	2.81	2.31	2.54	2.31	0.00

Figure 1. (a) Chemical structures of the molecules of interest. (b) Calculated excitation energies and singlet-triplet energy gaps (in eV). $E_v(S_0\text{-}S_1/T_1)$ denotes the vertical excitation energy from S_0 to S_1 / T_1; $E_a(S_0\text{-}S_1/T_1)$, the adiabatic excitation energy; and ΔE_{ST}, the adiabatic singlet-triplet energy gap. A schematic diagram of the potential energy surfaces related to the TADF process is illustrated in Figure S1 in the SI. The values in parentheses refer to the experimental data.

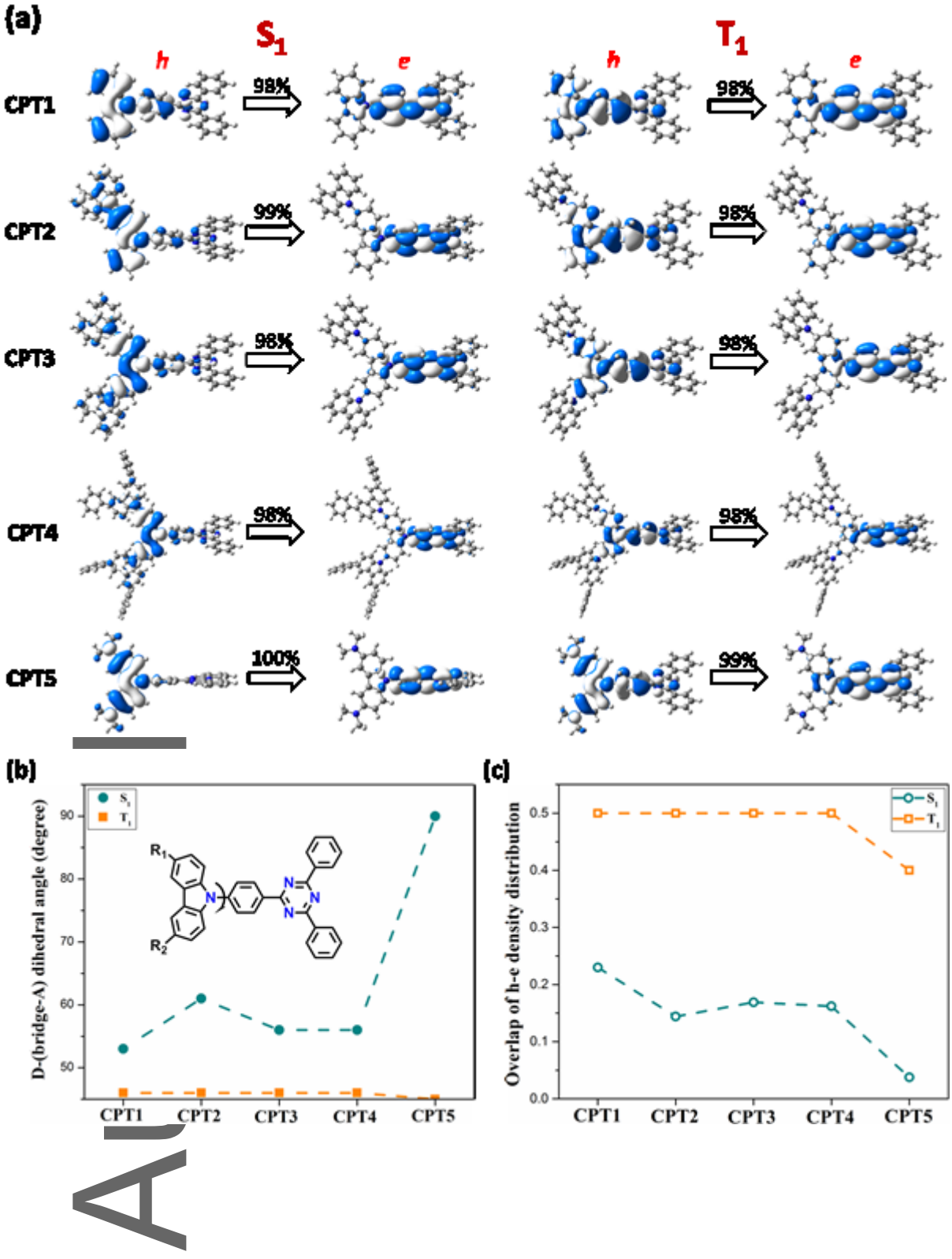

Figure 2. (a) Pictorial representation of natural transition orbitals (h: hole and e: electron) of the S_1 and T_1 states for the CPT1 – CPT5 molecules. The weight of the hole-electron contribution to the excitation is also included. (b) Dihedral angles (in degree) between the donor and bridge-acceptor moieties in the optimized S_1 and T_1 geometries. (c) Overlaps between the hole-electron (h-e) density distributions in the S_1 and T_1 states.

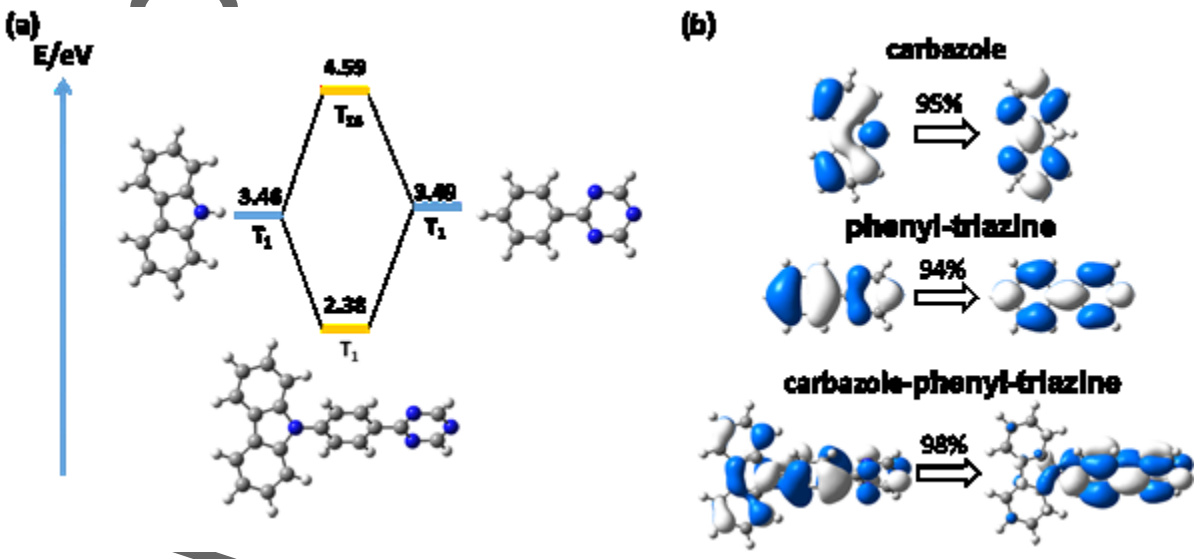

Figure 3. (a) Correlation diagram for the triplet states of the carbazole, phenylene-triazine and carbazole- phenylene-triazine fragments, based on the T_1 equilibrium geometry of CPT1. (b) Pictorial representation of the natural transition orbitals (NTO) for the T_1 states. The left and right sides show hole and electron wavefuntions, respectively. The weight of the hole-electron contribution to the excitation is also included.

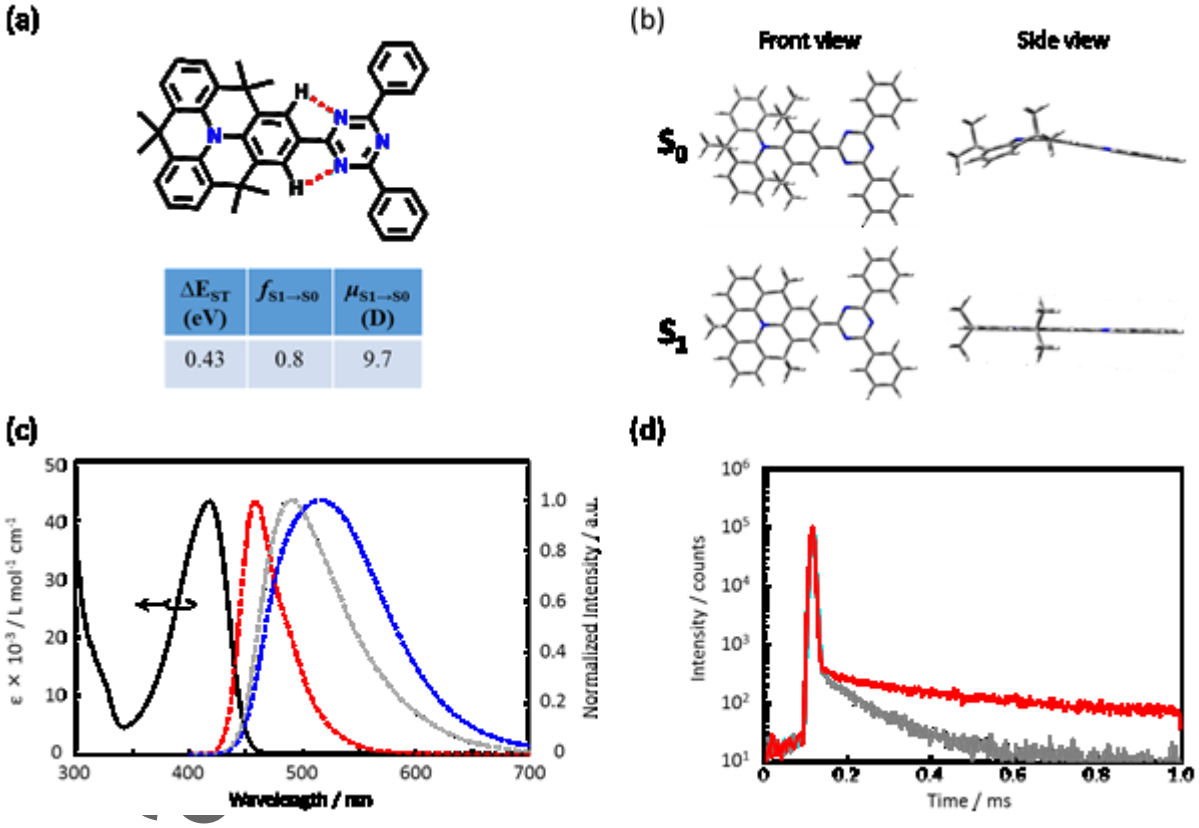

ΔE_{ST} (eV)	$f_{S1\rightarrow S0}$	$\mu_{S1\rightarrow S0}$ (D)
0.43	0.8	9.7

Figure 4. (a) Chemical structure of HMAT-TRZ (the red dashed line denotes the H-bonding interactions) and its TDDFT-calculated parameters related to the TADF process. (b) Optimized geometries in the S_0 and S_1 states. (c) UV/vis absorption (solid black line) and fluorescence spectra (dashed red line) in toluene solution (1×10^{-5} M), fluorescence spectra (dashed blue line) in chloroform (1×10^{-5} M), and fluorescence spectra (dashed gray line) of a 10 mol% HMAT-TRZ doped PMMA film. (d) Transient photoluminescence decay spectra of a 10 mol% HMAT-TRZ doped PMMA film under vacuum (red line) and ambient (gray line) conditions at 300 K.

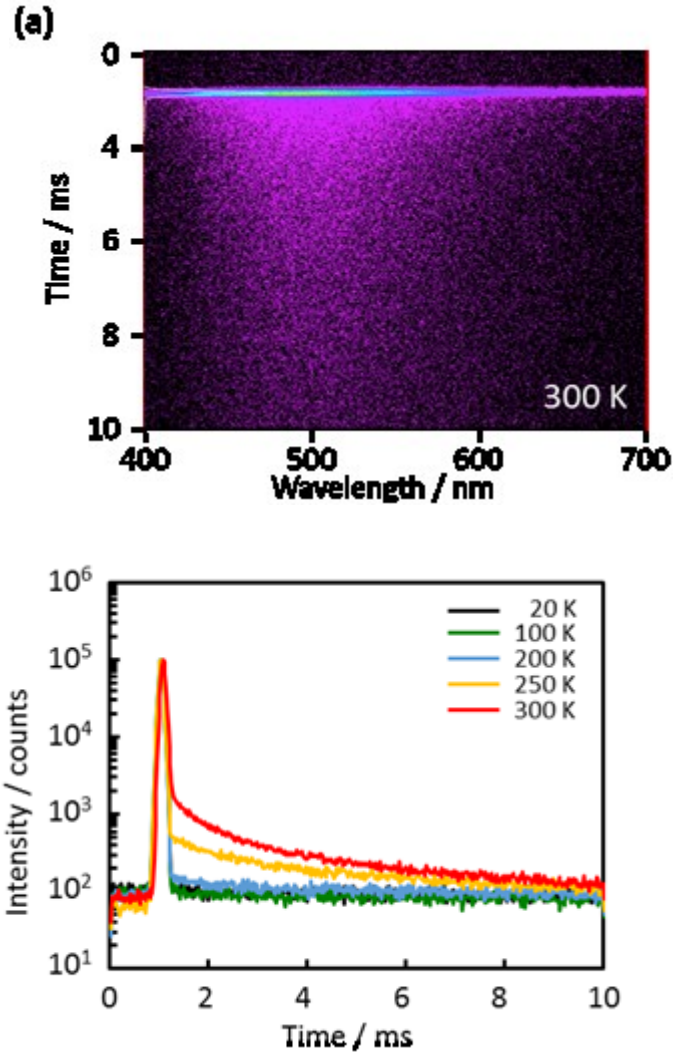

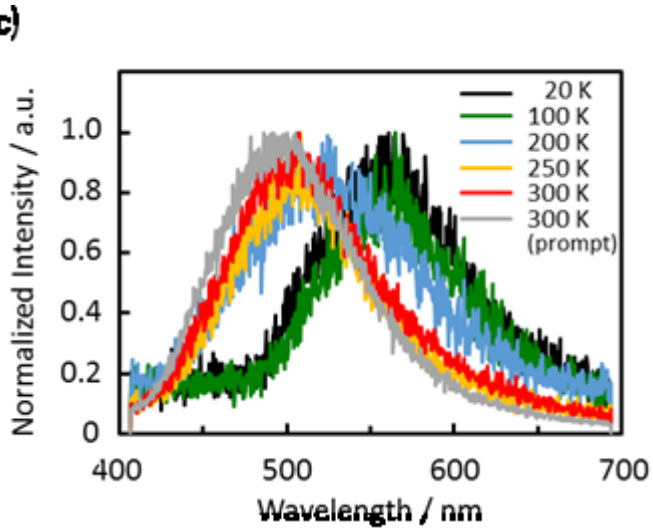

Figure 5. (a) Streak camera images (in 300 K); (b) temperature dependences of transient photoluminescence decay spectra; and (c) delayed spectra at various temperatures (gray line: prompt spectra and the lines with other colors: delayed spectra) for a HMAT-TRZ doped mCBP film (10 wt%).

Table 1. Calculated fluorescence oscillator strengths ($f_{S1\rightarrow S0}$), transition dipole moments ($\mu_{S1\text{-}S0}$), main electron configurations in the S_1 states and overlap between frontier molecular orbitals for the CPT1 – CPT4 series.

	$f_{S1\rightarrow S0}$	$\mu_{S1\text{-}S0}$ (Debye)	Electron configurations	Orbital overlap
CPT1	0.61	7.14	H → L: 89%	<H|L> = 0.32
CPT2	0.40	5.95	H → L: 75%; H-1 → L: 16%	<H|L> = 0.16; <H-1|L> = 0.04
CPT3	0.53	6.89	H → L: 77%; H-4 → L: 15%	<H|L> = 0.17; <H-4|L> = 0.33
CPT4	0.54	6.99	H → L: 74%; H-4 → L: 19%	<H|L> = 0.13; <H-4|L> = 0.32

A new strategy is proposed for the molecular design of efficient thermally activated delayed fluorescence (TADF) emitters that combine small singlet-triplet energy gaps and large fluorescence oscillator strengths. This strategy goes beyond the traditional framework of twisted TADF emitters and open the way for coplanar molecules to be efficient TADF emitters.

Keywords: thermally activated delayed fluorescence, molecular design, singlet-triplet energy gap, oscillator strength, planar structure

Xian-Kai Chen, Youichi Tsuchiya, Yuma Ishikawa, Cheng Zhong, Chihaya Adachi, and

Jean-Luc Brédas*

A New Design Strategy for Efficient Thermally Activated Delayed Fluorescence (TADF) Organic Emitters: From Twisted to Planar Structures

ToC figure